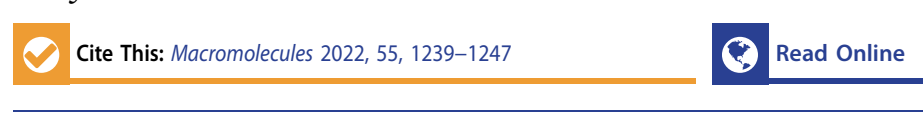
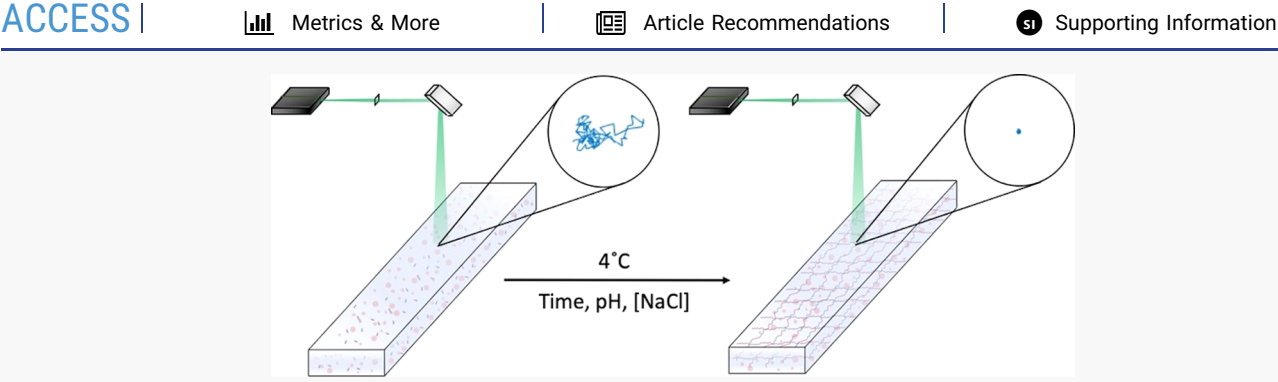


pubs.acs.org/Macromolecules Article

# High-Throughput Microrheology for the Assessment of Protein Gelation Kinetics

Michael Meleties, Dustin Britton, Priya Katyal, Bonnie Lin, Rhett L. Martineau, Maneesh K. Gupta, and Jin Kim Montclare\*





ABSTRACT: A high-throughput microrheological assay is employed to assess the gelation kinetics of a coiled-coil protein, Q, across a compositional space with varying ionic strengths and pH values. Two methods of passive microrheology—multiple particle tracking (MPT) and differential dynamic microscopy (DDM)—are used to determine mean-squared displacements of tracer beads embedded in protein solutions with respect to lag time over a fixed period. MPT data was analyzed to determine gelation kinetics in a high-throughput, automatable manner by fitting relaxation exponents to sigmoidal curves and verifying with the more traditionally used time-cure superposition. DDM-determined gelation time was assessed as the last resolvable time, which we found to be on a similar scale to gelation times given by MPT. Both methods show distinct advantages with regard to being used in a high-throughput, automatable setup; DDM can serve as an effective initial screen for rapid gelation kinetics due to it requiring less user intervention and inputs, with MPT giving a more complete understanding of the entire gelation process. Using these methods, a clear optimum for rapid gelation was observed near the isoelectric point of Q and at higher ionic strengths over the compositional space studied.

#### ■ INTRODUCTION

The ability to self-assemble in response to external stimuli makes protein biomaterials attractive for use in various biomedical applications. 1-4 In particular, protein biomaterials that are responsive to different physiological conditions, including temperature, pH, and ionic strength, can easily be adapted for applications where an in vivo hydrogel is desired. The self-assembly of proteins into higher-order structures is commonly associated with a change in a material's viscoelastic behavior,<sup>5</sup> particularly in the case of protein hydrogels.<sup>6</sup> Understanding the gelation kinetics and mechanisms of protein hydrogels is key in assessing their utility in biomedical applications and the design of future biomaterials; fast-gelling systems (<1 h) are considered to be clinically useful for in situ gelation for drug and/or gene delivery, while slower-gelling systems have been shown to be applicable in tissue engineering due to their potential to maintain cell viability and homogeneity throughout the matrix.8 Microrheology has previously been used to track changes in a material during its solution-to-gel (sol-gel) transition, with the critical

relaxation exponent having been shown to characterize the degree of connectivity in a percolated system and shifts in the relaxation exponent able to describe the overall sol—gel transition. Hadvantages of passive microrheology, including the use of small sample volumes and lack of user interaction during measurements, have made it a critical method for biomaterials research. Compared to active microrheology, where an external force is applied to drive tracer particle motion, 12–14 passive microrheology relies on the inherent thermal energy of the system, which allows multiple samples to be rapidly screened in high throughput. While passive microrheology has been previously used for protein-based materials to determine properties related to protein self-

Received: November 4, 2021 Revised: January 24, 2022 Published: February 9, 2022





assembly, dynamics, and protein—protein interactions, the method appears to be underutilized in the characterization of gelation kinetics of protein hydrogels and would be of interest for studies where libraries of proteins or conditions that can impact gelation are screened.  $^{15-19}$ 

Multiple particle tracking (MPT) is a form of passive microrheology that consists of tracking the movement of tracer beads through a sample or medium. The intensity profile of each particle is used to track the particles across frames and determine their mean-squared displacements (MSDs) at different lag times  $(\tau)$ . MPT has been used previously by Schultz et al. to determine the gelation regime of maleimidefunctionalized heparin hydrogels covalently cross-linked with dithiolized poly(ethylene glycol) over a large parameter space.<sup>20,21</sup> Similarly, Larsen *et al.* analyzed gelation kinetics of β-hairpin peptides using MPT.<sup>22</sup> Faster gelation kinetics were reported for peptides with point mutations that reduced the net charge of the peptide, as well as at increased ionic strengths.<sup>22</sup> In contrast to MPT, the more recently introduced differential dynamic microscopy (DDM) gives the ensemble average MSD by analyzing difference images generated from the pixel-by-pixel variations across image-pairs separated by a specific lag time. <sup>23–25</sup> DDM has been employed to characterize dynamics of protein-rich liquid clusters and correlate their results to those of dynamic light scattering. However, only Brownian motion has been characterized with no changes in the studied microenvironment's viscoelastic behavior over time.<sup>18</sup> While DDM has been gaining traction in the characterization of a number of biomaterials, 26 it has only recently started to be applied to hydrogels; a notable example is the recent use of DDM as a screen for the gelation of silk hydrogels, with data collection and analysis being automated and combined with machine learning algorithms to identify conditions that will lead to gelation in a desired time frame.<sup>27</sup> In this work, we perform passive microrheology in high throughput to compare different methods of analysis and identify an optimal set of conditions that results in gelation on the shortest time scale. We use a coiled-coil protein, Q, that is capable of upper critical solution temperature (UCST) phase behavior as a model system to track how its gelation is affected across a wide parameter space.

Previously, we characterized Q for its phase behavior in response to different environmental stimuli. 28,29 UCST behavior was demonstrated, with Q forming a hydrogel when cooled below its transition temperature.<sup>28</sup> Additionally, increased coiled-coil content and faster gelation kinetics were observed at pH levels close to the isoelectric point (pI = 10.3) of Q.29 These studies were now expanded in an effort to evaluate the gelation of Q at different pH values and ionic strengths by varying concentrations of sodium chloride. A high-throughput microrheological screen was used to rapidly evaluate phase behavior of Q for a library of conditions, with both MPT and DDM used in data analysis and assessed for their utility. Twenty-five total conditions were assessed in parallel, allowing gelation time to be assessed for the library at a much higher rate than if attempted through standard rheology. It was confirmed that faster gelation is observed near the isoelectric point, with a general trend of increased ionic strength also resulting in faster gelation for a constant pH. Furthermore, both MPT and DDM showed distinct advantages compared to each other, suggesting that a combination of the two methods would allow a complete analysis of phase behavior.

#### MATERIALS AND METHODS

Materials. M15MA Escherichia coli cells<sup>30</sup> were a gift from David Tirrell (California Institute of Technology). Tryptic soy agar, ampicillin sodium salt, kanamycin sulfate, sodium phosphate monobasic monohydrate (NaH2PO4·H2O), sodium phosphate dibasic anhydrous (Na<sub>2</sub>HPO<sub>4</sub>), ammonium chloride (NH<sub>4</sub>Cl), potassium phosphate monobasic (KH<sub>2</sub>PO<sub>4</sub>), sodium hydroxide (NaOH), dextrose monohydrate (D-glucose), magnesium sulfate (MgSO<sub>4</sub>), calcium chloride (CaCl<sub>2</sub>), isopropyl B-D-1-thiogalactopyranoside (IPTG), Tris-hydrochloride (Tris-HCl), Pierce bicinchoninic acid (BCA) assay kit, Pierce Snakeskin dialysis tubing with a 3.5 kDa molecular weight cutoff (MWCO), sodium dodecyl sulfate (SDS), and Molecular Probes FluoSpheres (1.0  $\mu$ m) were acquired from Thermo Fisher Scientific. Imidazole was purchased from Acros Organics. HiTrap immobilized metal affinity chromatography (IMAC) fast flow (FF) 5 mL columns for protein purification were acquired from Cytiva Life Sciences. Macrosep and Microsep advance centrifugal devices with a 3 kDa MWCO and 0.2  $\mu$ m syringe filters were purchased from Pall Corporation. 4-(Cyclohexylamino)-1butanesulfonic acid (CABS) and Amicon Ultra-0.5 centrifugal filter units with a 3 kDa MWCO were purchased from Merck Millipore. Acrylamide/bis solution (30%) 29:1 and natural polypeptide SDSpolyacrylamide gel electrophoresis (SDS-PAGE) standard were purchased from Bio-Rad. Borosilicate glass capillaries (0.2 mm × 2 mm × 50 mm) were acquired from VitroCom. Glass slides (1 mm ×  $25 \text{ mm} \times 75 \text{ mm}$ ) were acquired from Electron Microscopy Sciences. Fast-curing two-component epoxy was acquired from JB Weld.

Expression and Purification. Previously established protocols were used for the expression of Q protein.<sup>28</sup> Briefly, the pQE30/Q plasmid encoding for the Q protein and ampicillin resistance was transformed into chemically competent M15MA E. coli cells carrying the pREP4 plasmid, encoding for kanamycin resistance. A single colony was used to inoculate a starter culture, which was then used for larger-scale expression. Expression was done in M9 minimal medium supplemented with 200  $\mu g$  mL<sup>-1</sup> ampicillin and 34  $\mu g$  mL<sup>-1</sup> kanamycin. When the cell culture reached an optical density at 600 nm of ~0.7, expression was induced via the addition of IPTG to a final concentration of 200  $\mu g$  mL<sup>-1</sup> and cells were grown for an additional 3 h post induction. Cells were harvested and stored at -80 °C until purification. Cell pellets were resuspended and lysed in Buffer A (50 mM Tris-HCl, 500 mM NaCl, pH 8) and spun down to remove insoluble cell debris. Q protein was purified on a HiTrap IMAC FF 5 mL column saturated with cobalt(II) chloride. Protein was eluted against a gradient of increasing imidazole concentration from 10 to 500 mM using Buffer B (Buffer A, 500 mM imidazole). <sup>28,29</sup> Fractions were assessed for purity using 12% SDS-PAGE, with pure fractions dialyzed against Buffer A.

**Sample Preparation.** Following dialysis, Q was concentrated to 1 mg mL<sup>-1</sup> using centrifugal filters with an MWCO of 3 kDa. At 1 mg mL<sup>-1</sup>, Q was buffer-exchanged five times against the buffer conditions to be tested. Tested environmental conditions include 50 mM Tris—HCl at pH 6, 7.4, and 10 and 50 mM CABS at pH 11 and 12, with each pH having NaCl concentrations varied at 250, 375, 500, 750, and 1000 mM NaCl. When buffer exchange was completed, the protein was further concentrated to 12.6 mg mL<sup>-1</sup> (2 mM). Protein concentrations were confirmed by BCA assays.

Fluorescent tracer beads were mixed into Q protein at a final concentration of 1% v/v and final volumes of 30  $\mu$ L for each condition. Glass capillary tubes (0.2 mm × 2 mm × 50 mm) were loaded with ~20  $\mu$ L of solution through capillary action and arranged in arrays of five on glass slides. <sup>20</sup> Capillaries were sealed off to prevent sample evaporation and attached to the slide using fast-curing epoxy resin.

**Optical Microscopy.** Samples were imaged at 0 h, corresponding to the first measurement and again at discrete time points on a Leica DMI 4000 B inverted microscope equipped with a Leica DFC310 FX 1.4-megapixel camera. For each series, 300 frames were taken with a spacing of 0.037 s between each frame ( $\sim$ 27 frames s<sup>-1</sup>) at 40× magnification with 2 × 2 binning. Samples were observed until tracer

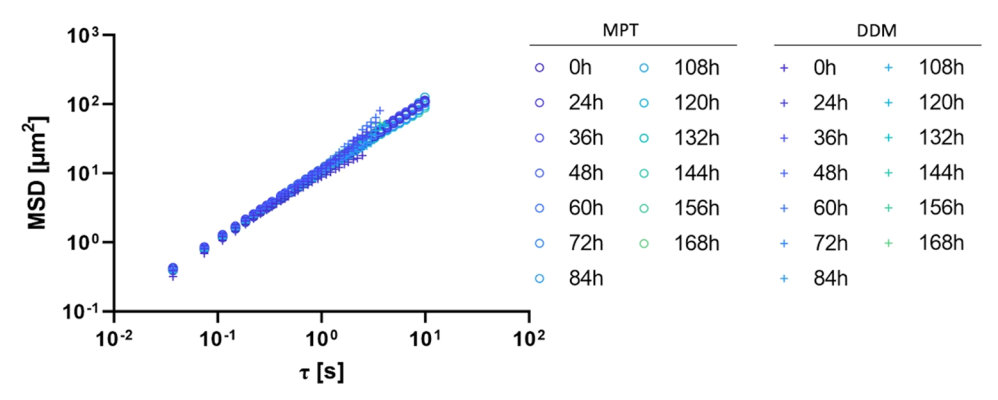


Figure 1. Log—log plot of MSD and lag time for Q at pH 6 and 500 mM NaCl, with no gelation or shift in relaxation exponent observed over 1 week. Open circles indicate MSDs determined using MPT and crosses indicate MSDs determined by DDM. Close agreement is observed at short lag times, with MSDs determined by DDM tailing upwards at longer lag times. Measurements were taken in triplicate, with a representative plot shown.

particle movement was no longer detectable or for a 1 week period if no change from initial particle movement was observed (indicating a nongelling sample). Between measurements, samples were kept at 4 °C on a lab rotisserie rotating at a rate of 8 rpm to prevent tracer particle sedimentation. Series of images were stacked and converted to grayscale in MATLAB (MathWorks, R2021a) using code developed in-house.

**Data Analysis.** Image stacks were analyzed using two different techniques: MPT and DDM.

Multiple Particle Tracking (MPT). MATLAB code developed and modified by Dufresene, Kilfoil, Blair, and O'Neill was adapted for MPT analysis, with further modifications for high-throughput capabilities. <sup>31–34</sup> The same intensity thresholds and feature-tracking parameters for data analysis were used in the analysis of all imaged samples and time points, which was justified based on observations of the optical properties of the gels remaining constant across all time points. Trajectories of tracer particles were tracked from frame to frame using their respective intensity profiles. Dedrifting algorithms were employed to minimize any average bulk motion observed for the particles. MSDs of single trajectories were averaged to give the ensemble average MSD with respect to lag times spanning up to the duration of each image series. <sup>35</sup>

MSDs determined through MPT were further analyzed to determine gelation times. Relaxation exponents (a) were determined for each time point by taking the logarithmic slope of the MSD– $\tau$  curves over the range of lag times studied (0.037–11.1 s). Slopes of ~1 indicate the Brownian motion of particles within a solution, while slopes <1 indicate subdiffusive behavior. <sup>36</sup> Gelation times were determined by fitting relaxation exponents to sigmoidal curves (eq 1) to find the inflection point, with the time to inflection taken as the gelation time for each condition; in the fitted equation  $\max_a$  and  $\min_a$  are the maximum and minimum relaxation exponents, respectively, during the gelation process, k is a kinetic gelation constant  $[h^{-1}]$ , and  $t_{\rm gel}$  is the time to gelation [h]

$$a = \max_{a} -(\max_{a} - \min_{a}) \frac{1}{1 + \exp(-k(t - t_{gel}))}$$
(1)

To validate the sigmoidal model used, gelation times were also determined using time-cure superposition. The initial MSD- $\tau$  curve at 0 h was treated as the master solution curve, with subsequent curves superimposed onto this curve. At the time which the data diverged, the remaining curves were instead superimposed onto the final MSD- $\tau$  curve, i.e., the master gel curve where bead movement was no longer detectable. Superposition was achieved by shifting intermediate curves horizontally by scaling the lag times with the relaxation time (horizontal) shift factor, a, and vertically by scaling the MSDs with the creep compliance (vertical) shift factor, b, which is discussed further below.

Differential Dynamic Microscopy (DDM). Image stacks were also analyzed through DDM in MATLAB using code developed and available online in the form of DDMCalc (v1.0) by Bayles et al.<sup>38</sup> For the entire image stack, difference images were generated from the differences in pixel intensities of pairs of images for specific lag times. The image structure function was then generated from the average value of the squared modulus of the Fourier-transformed image differences for each respective lag time in the image series.

MSDs were generated from the image structure function according to protocols outlined by Bayles et al. using a standard deviation cutoff of 0.025 au, which is the only user-defined threshold in the DDM analysis used herein.<sup>39</sup> Contributions of the Fourier-transformed probe intensity profile and incoherent background signal were determined from the image structure function by analyzing its longand short-term limits.<sup>39</sup> Specifically, the incoherent background signal was determined as the value of the image structure function as the lag time approached 0.39 The long-term plateau of the image structure function is the sum of the two contributions, which allows for the Fourier-transformed probe intensity profile to then be determined by subtracting the background contribution from the long-term plateau.<sup>39</sup> Large displacements at long lag times and high wave vector (q) values were excluded from MSD calculations by only considering lag times where the image structure function is less than 80% of its long-term plateau.<sup>39</sup> Because MSDs become increasingly difficult to resolve from the image structure function as the particle movement becomes hindered, the gelation time could not be determined in the same way as was done for MPT-determined MSDs, namely, using time-cure superposition or fitting results to a sigmoidal curve. Instead, for gel time estimates based on DDM in this work, the last observation time in a gelling reaction wherein DDM could be used to resolve MSDs was taken as an estimate of the gel time. This approach has been used recently to study gelation in silk hydrogels with embedded bacteria, enabling the characterization of a large formulation space in terms of the likelihood of gelation based on formula constituency.<sup>2</sup>

# ■ RESULTS AND DISCUSSION

# Mean-Squared Displacement of Tracer Particles over

**Time.** MPT and DDM were each employed to determine the MSD of inert tracer particles as a function of lag time. User-defined intensity thresholds that were used for MPT analysis were confirmed for each series of images to predominantly accept beads that were in focus of the objective lens (Figure S1), with the settings kept constant across each sample. Gelation kinetics of Q were investigated across a range of different ionic strengths and pH levels. We previously demonstrated that the self-assembly of Q near its isoelectric point results in faster gelation and an increased elastic

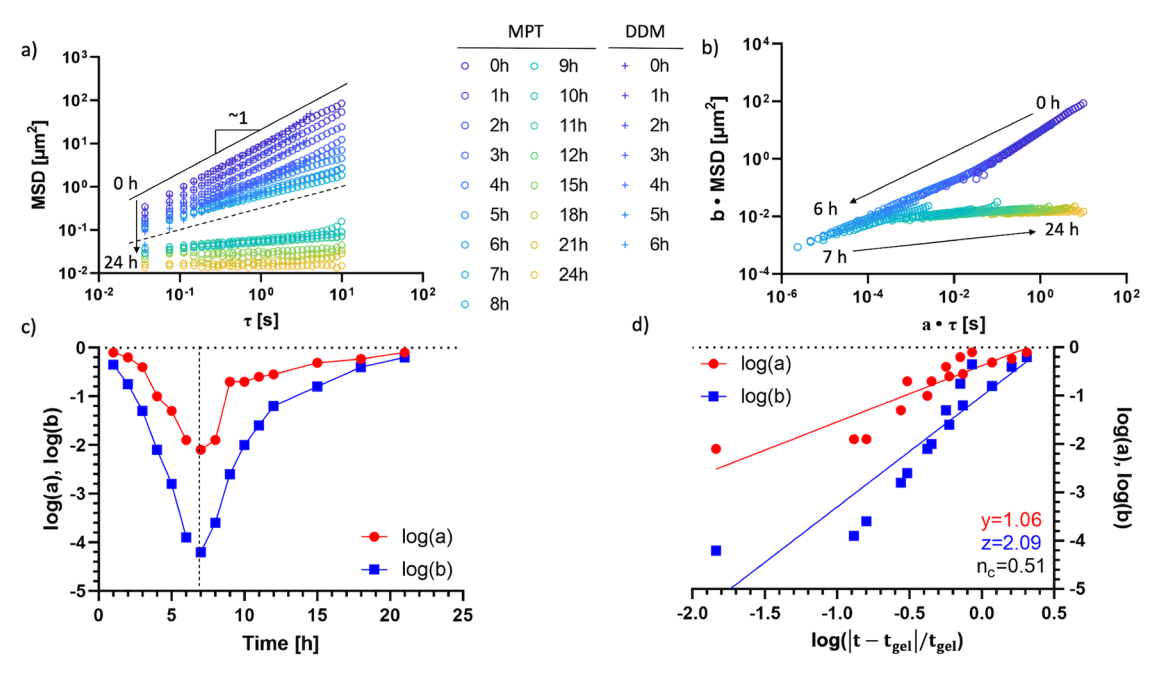


**Figure 2.** (a) Log-log plot of MSD and lag time for Q at pH 10 and 500 mM NaCl. Values determined by MPT and DDM are indicated as open circles and crosses, respectively. Solid and dashed reference lines have slopes of 1 and 0.5, respectively. (b) Time-cure superposition of MSD and lag time for MPT-determined measurements in panel (a) using lag time scaled by a horizontal shift factor, a, and MSD scaled by a vertical shift factor, b. (c) Logarithm of horizontal and vertical shift factors plotted as a function of time to determine the time to gelation (determined to be 6.9 h in sample case). (d) Log-log plot of shift factors and distance from critical time to gelation. Logarithmic slopes of the shift factors are used to determine the critical relaxation exponent. All measurements and analyses were made in triplicate, with representative plots shown.

modulus.<sup>29</sup> A high-throughput microrheological assay was applied to determine gelation times across a pH range of 6-12 and a range of NaCl concentrations from 250 to 1000 mM. At pH 6, Q was not able to form a hydrogel at any of the studied ionic strengths (Figure 1). This was consistent with earlier findings that suggested that electrostatic repulsions created by the net-positive charge of the protein at pH 6 prevent fiber assembly and subsequent gelation.<sup>29</sup> On a log-log plot, MSDs determined by MPT and DDM each retained a linear relationship with lag time over a 1 week period with a logarithmic slope of  $\sim 1$  (Figures 1 and S2), consistent with the Brownian motion of the tracer particles. For samples that were able to form a hydrogel, including Q at pH 7.4-12 and all ionic strengths studied, curves with slopes characteristic of Brownian motion were observed at initial time points, followed by the onset of subdiffusive behavior at subsequent time points (a < 1) (Figure 2a). As the sample continued to gel, its relaxation exponent continued to decrease to the point where it no longer scaled, or very weakly scaled, with lag time (0 < a) $\ll$  1). At time points where there was no further decrease in MSD, the gelation process was deemed to be complete.

**Time-Cure Superposition.** Gelation kinetics are initially assessed using time-cure superposition, as has been the traditionally used method for the determination of gelation times.  $^{9,28,32,36}$  For each sample,  $MSD-\tau$  curves on a log-log plot are empirically superimposed at different extents of gelation onto the master solution curve and master gel curve, which is the 0 h time point and final time point, respectively (Figure 2b). The master solution curve indicates the observed Brownian motion of the tracers, while the master gel curve is the final time point where further decreases in the scaling of MSD with lag time are not detectable. Intermediate curves are initially superimposed onto the master solution curve by shifting the  $MSD-\tau$  curves horizontally using the horizontal

shift factor, a, and vertically using the vertical shift factor, b. The horizontal and vertical shift factors scale the lag time and MSD, respectively, and are related to the distance from the critical extent of gelation and the critical gelation time. Superposition was deemed to be complete when maximal overlap was observed between MSD- $\tau$  curves and shift factors and distance from the critical extent of gelation were linear on a log-log scale. Gelation time is determined by the asymptotic behavior of the two shift factors as they approach the critical gelation time (Figure 2c). Time-cure superposition curves have also been used to identify the critical relaxation exponent from the time where pre- and postgelation curves converge (Figure 2d). Critical relaxation exponents can be related to the degree of cross-linking of the system, with  $n_c$  < 0.5 being indicative of densely cross-linked systems and  $n_c > 0.5$  indicative of loosely cross-linked system.<sup>36</sup> Critical relaxation exponents across all conditions studied for Q are between 0.4 and 0.6 (Table S1), which has previously been shown for physically cross-linked biomaterial systems.  $^{9,28,40-42}$ 

**Sigmoidal Curve-Fitting.** As time-cure superposition of MSD- $\tau$  curves is done empirically, it is not suitable for high-throughput analysis. To save time and eliminate user-bias, an automatable analysis method to determine the gelation time and critical relaxation exponent is implemented, where the slopes of MSD- $\tau$  curves are fit to sigmoidal curves. The relaxation exponent during the gelation process normally includes a short- and long-term plateau with respect to time and a transition from solution to gel where the relaxation exponent rapidly drops, overall following a sigmoidal-like curve. The short-term plateau indicates the solution slowly becoming more viscous, and the long-term plateau represents the sample's relaxation exponent equilibrating to a final value. Thus, data is fit to a sigmoidal curve (eq 1), where the gelation time is determined as the time of the inflection point. Criteria

for fitting of the sigmoidal curve are described in the Supporting Information. In brief, criteria have been set where fitted models have physically relevant constants, avoiding negative times to gelation. Results of sigmoidal curve-fitting largely fit the relaxation exponent changes over time well for all conditions studied, fitting particularly well ( $r^2 > 0.9$ ) for pH 10–12 (Figures 3 and S3–S6 and Table S2).

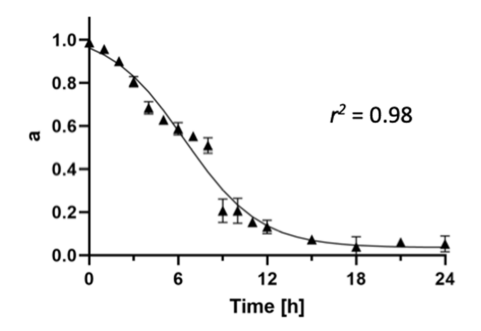


Figure 3. Relaxation exponents for Q at pH 10, 500 mM NaCl over time. Relaxation exponents were fit to a sigmoidal curve, indicated by the solid line. Error bars, which represent standard deviation, are shown for an average of three trials; points without error bars had standard deviations that were too small to be shown.

Gelation times determined through sigmoidal fits agree with values determined through time-cure superposition, with differences not being statistically significant as determined by a two-way analysis of variance (ANOVA) test (Table S3). At pH 7.4, Q exhibits gelation similar to that of previously published results at pH 8. Specifically, at 500 mM NaCl, Q demonstrates a gelation time of  $75.0 \pm 4.7$  h, compared to that of 70.4  $\pm$  0.1 h at pH 8.28 At pH 10-12, gelation for all samples occurs in less than 24 h. Q reveals the fastest gelation at pH 10 and a NaCl concentration of 1000 mM, forming a hydrogel in  $0.9 \pm 0.6$  h. For each pH level, there is a general trend of faster gelation with increasing NaCl. This can be attributed to the increased screening of long-distance electrostatic repulsions, allowing for an increased effect of short-term electrostatic interactions occurring between charged patches on the surface of Q, resulting in coiled-coil stacking and selfassembly into fibers, which then physically cross-link to form hydrogels.<sup>29</sup> Previous studies into the morphology of the Q hydrogel at pH 8, 500 mM NaCl revealed pore sizes of 123.7  $\pm$ 26.6 nm, <sup>28</sup> well below the 1  $\mu$ m sized particles used as tracers here. While the results of sigmoidal curve-fitting agree with those of time-cure superposition in this case, it is important to note that the inflection point is not always synonymous with the critical extent of gelation, as shown by Bilge and Pekcan who instead used the limit where derivatives of the gelation curves reach their extreme values to characterize the gelation time.43 Instead, it has previously been suggested that the inflection point agrees with the gelation time for cases where the critical relaxation exponent is  $\sim 0.5$ , 44 as is the case here.

pH and lonic Strength Impact on Gelation. The high-throughput screening and high-throughput analysis of multiple environmental conditions (pH and ionic strength) allow for the rapid generation of a map of times to gelation over the entire compositional space studied (Figure 4). This map shows the times to gelation obtained from sigmoidal curve-fitting analysis of MSD– $\tau$  curves determined through MPT. Warm colors indicate shorter times to gelation and more rapid gelation kinetics, whereas cooler colors indicate much longer

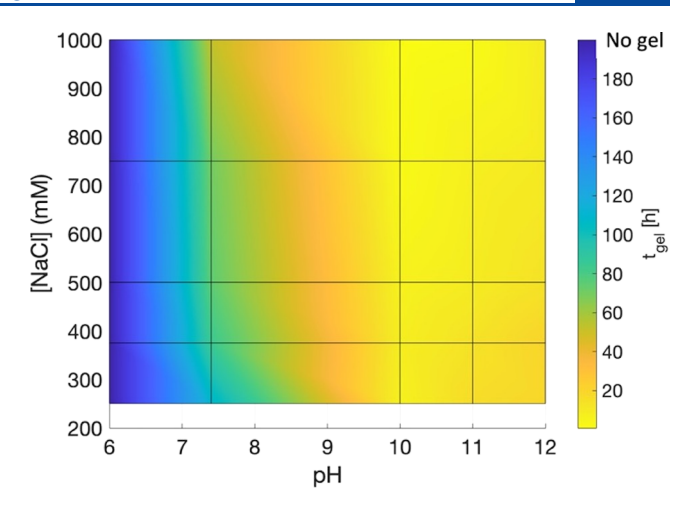


Figure 4. Surface plot of gelation times determined by sigmoidal curve-fitting of MPT-determined MSDs for the entire compositional space studied. Values shown for each condition are averaged from three independently prepared samples. Short times to gelation are indicated by warmer colors, while long times to gelation (or failure to gel) are indicated by cooler colors. Intersections of lines in the plot indicate combinations of pH and ionic strength where gelation time was experimentally determined.

times to gelation or slow gelation kinetics. The maximum for this map, indicated in dark blue, occurs for all ionic strengths studied at pH 6, where gelation is not observed; no change in relaxation exponent and thus viscoelastic behavior of the sample, in general, is observed for pH 6.

As the pH of 10–12 showed gelation times on a much faster scale compared to pH 7.4, their gelation kinetics were further analyzed by plotting the evolution of their respective relaxation exponents at the ionic strengths studied (Figure 5). The map for the initial time point revealed a mostly uniform cool map, demonstrating the initial solution state of the protein for all conditions studied. After 3 h, the relaxation exponent for pH 10 and 1000 mM NaCl dropped to 0.21  $\pm$  0.01, which was well below its critical relaxation exponent, confirming the solgel transition; this was a clear optimum for rapid gelation kinetics among the conditions studied. Assessment of the maps for the remaining time points demonstrated gelation occurring across the compositional space, with a clear "gelation front" moving from high ionic strength near the isoelectric point to lower ionic strength further from the isoelectric point. At the 48 h time point (Figure S7), the compositional space between pH 10 and 12 exhibited relaxation exponents across all ionic strengths that were consistent with equilibrated gelation states for Q.

Particle Trajectories and Heterogeneity of Microenvironments. Through MPT analysis, insight into the transition of the microenvironment during gelation can be attained. Visual inspection of randomly selected bead trajectories at different time points shows similar MSDs on the same order of magnitude compared to other trajectories in the same sample (Figure 6). Over time, the MSDs consistently get confined to smaller areas due to increased cross-linking by the fibrous network with their trajectories resulting in small dot sizes relative to their initial trajectories. Across all samples that are able to form hydrogels, a decrease in MSD is observed.

To assess the heterogeneity of the microenvironment, the non-Gaussian parameter (N) of the van Hove correlation function was calculated pre- and postgelation for one-

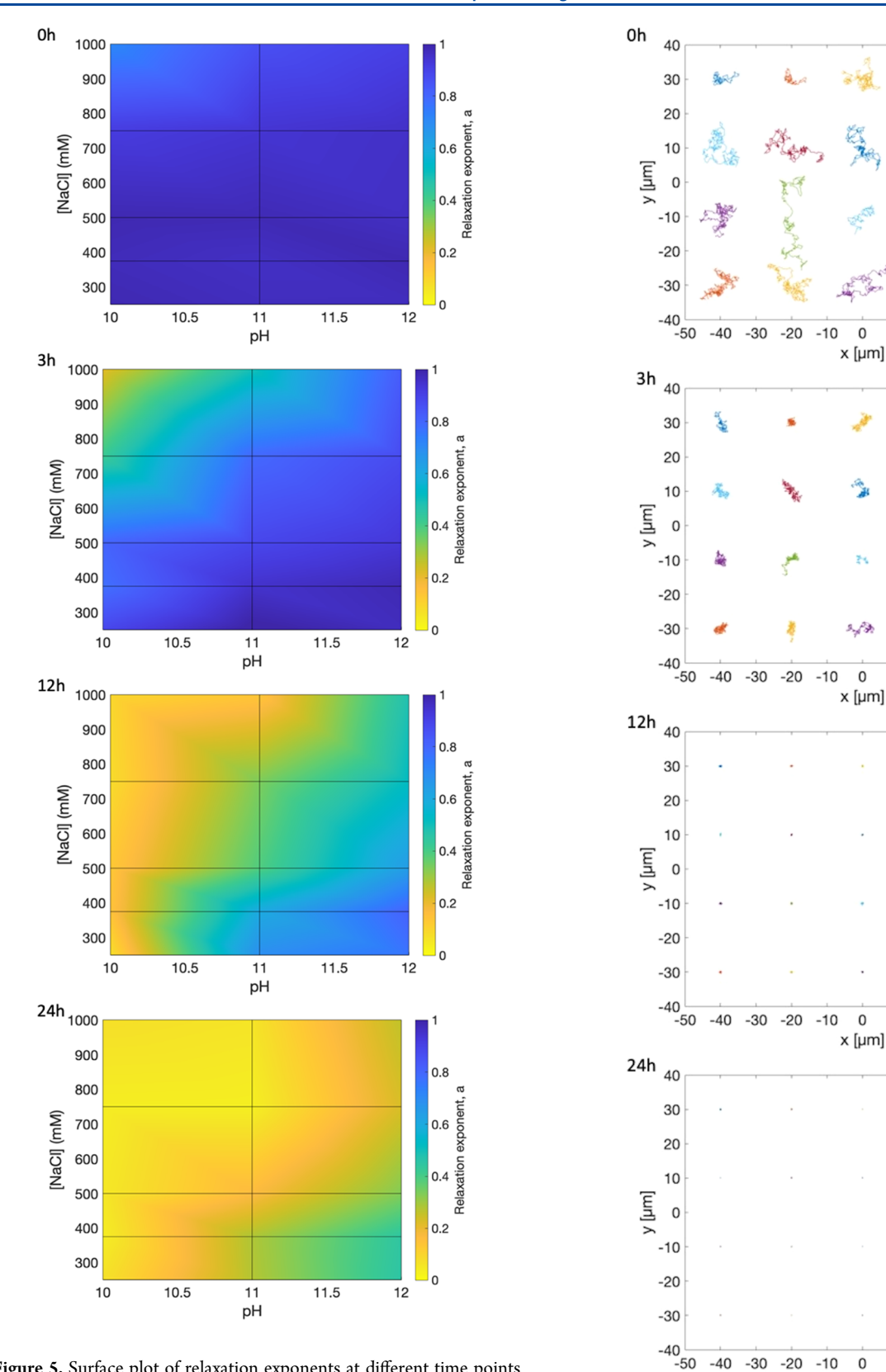


Figure 5. Surface plot of relaxation exponents at different time points for MSDs determined through MPT for all ionic strengths studied for Q at pH 10–12. Values shown for each condition are averaged from three independently prepared samples. Cool colors represent relaxation exponents near 1, indicating a solution, while warm colors represent relaxation exponents closer to 0, indicating a hydrogel. Intersections of lines in the plot indicate combinations of pH and ionic strength where relaxation exponents were experimentally determined.

**Figure 6.** Particle trajectories of tracer beads embedded in Q at pH 10, 500 mM NaCl at 0, 3, 12, and 24 h. Axes represent arbitrary positions in units of  $\mu$ m. Decreasing MSD of the tracer beads is observed over time due to gelation. For each panel, 20 trajectories were randomly selected from a representative sample.

10 20 30 40 50

10 20 30 40

10 20 30 40

10 20 30 40

x [µm]

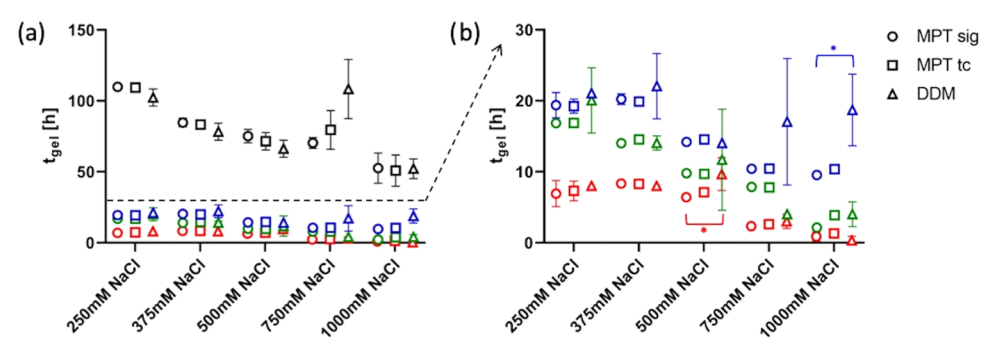


Figure 7. (a) Comparison of gelation times determined by MPT through fitting to a sigmoidal (MPT sig), through time-cure superposition (MPT tc), and determined by DDM as the last time where the image structure function was resolvable for pH 7.4 (black), pH 10 (red), pH 11 (green), and pH 12 (blue) at different ionic strengths. (b) Gelation times pH 10–12 plotted on a separate set of axes for better visualization of data trends. For each combination of pH and ionic strength, differences in the results of the three methods were shown to not be statistically significant as determined by a two-way ANOVA test, with the exception of pairs indicated by \*. Error bars represent standard deviation for an average of three trials. Samples without error bars had standard deviations that were too small to be shown.

dimensional trajectories over a lag time of 1.1 s. 45,46 As done previously, particle displacements in the x- and y-directions were averaged for improved statistics.<sup>45</sup> The non-Gaussian parameter is 0 for a Gaussian distribution, and deviation from this value indicates a heterogeneous microenvironment.<sup>47</sup> Q samples at pH 6 did not show increases in heterogeneity over the time period studied (Table S4), which is consistent with no change in the microenvironment being probed. By contrast, non-Gaussian parameters showed order-of-magnitude increases after gelation for Q at pH 7.4-12, suggesting an increase in microenvironment heterogeneity (Table S4). For the trajectories of Q at pH 10 and 500 mM NaCl shown in Figure 6, the non-Gaussian parameter increased from 0.046  $\pm$ 0.007 at 0 h to 0.843  $\pm$  0.080 at 24 h, showing an increase in heterogeneity of the microenvironment being probed by the tracer particles following gelation.

Comparison of Multiple Particle Tracking and Differential Dynamic Microscopy. MPT and DDM are in close agreement between determined MSDs for samples where the image structure function is resolvable. For pH 6, where Q does not form a gel, both DDM and MPT reveal a constant slope of ~1 throughout the time period where measurements are being collected (Figures 1a and S2). The relaxation exponents given by MPT and DDM agree in the short-term response  $(\tau \to 0)$ but begin to deviate at long-term lag times. A possible reason for this may be stage drift that is present and may create uniaxial motion; this would have an effect on particle movement that only becomes apparent at later response times since the particles' individual motion would dominate at shorter response times. 48 Dedrifting algorithms have previously been written for MPT and are commonly employed as done so here, whereas DDM is still a relatively new technique and advancements in dedrifting have only recently been made. 49,50 For samples that undergo gelation, MSDs determined by MPT and DDM agree at time points prior to the critical gelation point. Some deviation from the MSDs measured by MPT is also observed at the long-term response for DDM, demonstrated by an uptick in the slope toward the end of the measurement. Furthermore, as the particle motion continues to be restricted to a greater extent during gelation, particle movement becomes more difficult to resolve from incoherent background noise, resulting in the image structure function failing to be resolved into MSDs after a certain extent of gelation.

Although not producing enough data to be fit to sigmoidal curves, we note that DDM normally fails to resolve the MSDs near the MPT-determined critical relaxation exponent. This suggests, in agreement with an earlier study employing DDM for gel time estimation,<sup>27</sup> that a possible way to screen for gelation using DDM is to equate the gelation time to the first time point where the image structure function is not resolvable using DDM. Gelation times determined through the sigmoidal fitting of MPT-determined MSDs, time-cure superposition of MPT-determined MSDs, and last resolvable times for DDM largely did not show any statistically significant difference. Only two conditions of the 60 analyzed yield p-values < 0.05 both showing an overestimated DDM-determined gelation time compared to sigmoidal-fitted gelation times—when analyzed using a two-way ANOVA test (Figure 7 and Tables S3 and S5). While not statistically different, it is important to note that the resolution failure times from DDM are prone to larger standard deviations in the data compared to those for either analysis method used with MPT. As the relationship between the critical relaxation exponent of a gelling system and the time at which DDM tends to fail to resolve the MSDs is not generally known, DDM should only be used in a screening capacity or to approximate gel times in complex systems where the critical relaxation exponent (if desired) can be confirmed by MPT. This renders MPT an indispensable method when analyzing gelation kinetics of a protein hydrogel. Still, DDM can remain an effective tool for the initial screening of gelation, particularly when employed in high throughput, due to its lack of user inputs compared to MPT. DDM also remains attractive as an initial screening tool due to its robustness in being used for a variety of samples. In our case, the optical properties of the sample did not change with time, allowing for the use of the same MPT settings for each sample and for each time point. However, there are many examples, such as elastin-likepolypeptide-based and silk-based hydrogels whose phase transition is accompanied by a shift in turbidity to an opaque white.<sup>27,51</sup> While MPT would require user intervention to reoptimize thresholds and parameters used for analysis, DDM analysis would not require any changes in user-defined inputs. Thus, a suggested combination of the two methods for highthroughput material characterization would include an initial screen be done through DDM, prior to selecting promising candidates to further analyze using MPT.

#### CONCLUSIONS

Manipulation of gelation kinetics and mechanisms will expand the capabilities of protein hydrogels to multiple biomedical applications. As the assay employed here has a setup time greater than 5 min and is dependent on the total number of samples to be screened, systems with time to gelation greater than 30 min are more amenable to being studied than fastergelling systems. Alternatively, this assay can be used for fastgelling systems that have an external trigger for gelation, allowing the gelation process to be initiated once setup is complete. For the system studied here, gelation occurs on a much shorter time scale at pH levels near the isoelectric point and for higher ionic strengths compared to pH further from the isoelectric point and lower ionic strengths. This information can be leveraged in the design of future protein biomaterials with specific self-assembly properties in mind. To characterize gelation kinetics and self-assembly behavior in high throughput, passive microrheology is well positioned to be an increasingly used method for protein engineers. In this paper, the suitability of two passive microrheology techniques is assessed for characterizing gelation kinetics of Q. MPT can track tracer particle movement throughout the entire gelation process and reveals information about its heterogeneity; however, it may not always be suitable if the optical properties of the sample evolve over time such as shifts to opaque colors where tracer particles are not as easily resolvable using intensity thresholds. DDM presents a more robust method for analyzing samples regardless of optical properties but is limited in tracking gelation due to its inability to resolve MSDs of the probe particles as their movement becomes hindered. Thus, a combination of the two methods can be ideal for the screening of a library of samples or conditions, where DDM can be applied as an initial screen to determine which samples are showing the fastest gelation kinetics and MPT being applied to fully elucidate the gelation kinetics and mechanism once desired candidates or conditions have been identified.

# ASSOCIATED CONTENT

# Supporting Information

The Supporting Information is available free of charge at https://pubs.acs.org/doi/10.1021/acs.macromol.1c02281.

Description of the sigmoidal curve-fitting criteria, pretracking image demonstrating optimized MPT settings, sigmoidal models of relaxation exponents over time, and tables of critical relaxation exponents, fitted parameters for sigmoidal fits, non-Gaussian parameters, and *p*-values from statistical analysis (PDF)

#### AUTHOR INFORMATION

### **Corresponding Author**

Jin Kim Montclare — Department of Chemical and Biomolecular Engineering, New York University Tandon School of Engineering, Brooklyn, New York 11201, United States; Department of Radiology, New York University Langone Health, New York, New York 10016, United States; Department of Biomaterials, New York University College of Dentistry, New York, New York 10010, United States; Department of Chemistry, New York University, New York, New York 10003, United States; ◎ orcid.org/0000-0001-6857-3591; Email: montclare@nyu.edu

#### **Authors**

Michael Meleties — Department of Chemical and Biomolecular Engineering, New York University Tandon School of Engineering, Brooklyn, New York 11201, United States

**Dustin Britton** – Department of Chemical and Biomolecular Engineering, New York University Tandon School of Engineering, Brooklyn, New York 11201, United States

Priya Katyal — Department of Chemical and Biomolecular Engineering, New York University Tandon School of Engineering, Brooklyn, New York 11201, United States; orcid.org/0000-0003-3066-3537

Bonnie Lin – Department of Chemical and Biomolecular Engineering, New York University Tandon School of Engineering, Brooklyn, New York 11201, United States

Rhett L. Martineau – Materials and Manufacturing Directorate, Air Force Research Laboratory, Wright-Patterson Air Force Base, Ohio 45433, United States

Maneesh K. Gupta – Materials and Manufacturing Directorate, Air Force Research Laboratory, Wright-Patterson Air Force Base, Ohio 45433, United States

Complete contact information is available at: https://pubs.acs.org/10.1021/acs.macromol.1c02281

# **Author Contributions**

All authors have given approval to the final version of the manuscript.

# **Funding**

This work was supported by NSF-DMREF under Award Number DMR 1728858 and NSF-MRSEC Program under Award Number DMR 1420073.

#### Notes

The authors declare no competing financial interest.

#### ACKNOWLEDGMENTS

This work was supported, in part, through the NYU IT High Performance Computing resources, services, and staff expertise

#### REFERENCES

- (1) Banta, S.; Wheeldon, I. R.; Blenner, M. Protein Engineering in the Development of Functional Hydrogels. *Annu. Rev. Biomed. Eng.* **2010**, *12*, 167–186.
- (2) Katyal, P.; Mahmoudinobar, F.; Montclare, J. K. Recent trends in peptide and protein-based hydrogels. *Curr. Opin. Struct. Biol.* **2020**, 63, 97–105.
- (3) Katyal, P.; Meleties, M.; Montclare, J. K. Self-Assembled Proteinand Peptide-Based Nanomaterials. *ACS Biomater. Sci. Eng.* **2019**, *5*, 4132–4147.
- (4) Kopeček, J.; Yang, J. Smart Self-Assembled Hybrid Hydrogel Biomaterials. *Angew. Chem., Int. Ed.* **2012**, *51*, 7396–7417.
- (5) Tu, R. S.; Breedveld, V. Microrheological detection of protein unfolding. *Phys. Rev. E* **2005**, *72*, No. 041914.
- (6) Dooling, L. J.; Buck, M. E.; Zhang, W.-B.; Tirrell, D. A. Programming Molecular Association and Viscoelastic Behavior in Protein Networks. *Adv. Mater.* **2016**, *28*, 4651–4657.
- (7) Van Tomme, S. R.; Storm, G.; Hennink, W. E. In situ gelling hydrogels for pharmaceutical and biomedical applications. *Int. J. Pharm.* **2008**, *355*, 1–18.
- (8) Growney Kalaf, E. A.; Flores, R.; Bledsoe, J. G.; Sell, S. A. Characterization of slow-gelling alginate hydrogels for intervertebral disc tissue-engineering applications. *Mater. Sci. Eng., C* **2016**, *63*, 198–210.

- (9) Larsen, T. H.; Furst, E. M. Microrheology of the Liquid-Solid Transition during Gelation. *Phys. Rev. Lett.* **2008**, *100*, No. 146001.
- (10) Waigh, T. A. Microrheology of complex fluids. Rep. Prog. Phys. 2005. 68, No. 685.
- (11) Waigh, T. A. Advances in the microrheology of complex fluids. *Rep. Prog. Phys.* **2016**, *79*, No. 074601.
- (12) Efremov, Y. M.; Okajima, T.; Raman, A. Measuring viscoelasticity of soft biological samples using atomic force microscopy. *Soft Matter* **2020**, *16*, 64–81.
- (13) Yao, A.; Tassieri, M.; Padgett, M.; Cooper, J. Microrheology with optical tweezers. *Lab Chip* **2009**, *9*, 2568–2575.
- (14) Zia, R. N. Active and Passive Microrheology: Theory and Simulation. *Annu. Rev. Fluid Mech.* **2018**, *50*, 371–405.
- (15) Regan, K.; Wulstein, D.; Rasmussen, H.; McGorty, R.; Robertson-Anderson, R. M. Bridging the spatiotemporal scales of macromolecular transport in crowded biomimetic systems. *Soft Matter* **2019**, *15*, 1200–1209.
- (16) Escobedo-Sánchez, M. A.; Segovia-Gutiérrez, J. P.; Zuccolotto-Bernez, A. B.; Hansen, J.; Marciniak, C. C.; Sachowsky, K.; Platten, F.; Egelhaaf, S. U. Microliter viscometry using a bright-field microscope: η-DDM. *Soft Matter* **2018**, *14*, 7016–7025.
- (17) Haghpanah, J. S.; Yuvienco, C.; Roth, E. W.; Liang, A.; Tu, R. S.; Montclare, J. K. Supramolecular assembly and small molecule recognition by genetically engineered protein block polymers composed of two SADs. *Mol. BioSyst.* **2010**, *6*, 1662–1667.
- (18) Safari, M. S.; Vorontsova, M. A.; Poling-Skutvik, R.; Vekilov, P. G.; Conrad, J. C. Differential dynamic microscopy of weakly scattering and polydisperse protein-rich clusters. *Phys. Rev. E* **2015**, 92, No. 042712.
- (19) Zhou, Y.; Li, B.; Li, S.; Ardoña, H. A. M.; Wilson, W. L.; Tovar, J. D.; Schroeder, C. M. Concentration-Driven Assembly and Sol–Gel Transition of  $\pi$ -Conjugated Oligopeptides. *ACS Cent. Sci.* **2017**, 3, 986–994.
- (20) Schultz, K. M.; Baldwin, A. D.; Kiick, K. L.; Furst, E. M. Rapid rheological screening to identify conditions of biomaterial hydrogelation. *Soft Matter* **2009**, *5*, 740–742.
- (21) Schultz, K. M.; Furst, E. M. Microrheology of biomaterial hydrogelators. *Soft Matter* **2012**, *8*, 6198–6205.
- (22) Larsen, T. H.; Branco, M. C.; Rajagopal, K.; Schneider, J. P.; Furst, E. M. Sequence-Dependent Gelation Kinetics of  $\beta$ -Hairpin Peptide Hydrogels. *Macromolecules* **2009**, *42*, 8443–8450.
- (23) Cerbino, R.; Cicuta, P. Perspective: Differential dynamic microscopy extracts multi-scale activity in complex fluids and biological systems. *J. Chem. Phys.* **2017**, *147*, No. 110901.
- (24) Cerbino, R.; Trappe, V. Differential Dynamic Microscopy: Probing Wave Vector Dependent Dynamics with a Microscope. *Phys. Rev. Lett.* **2008**, *100*, No. 188102.
- (25) Edera, P.; Bergamini, D.; Trappe, V.; Giavazzi, F.; Cerbino, R. Differential dynamic microscopy microrheology of soft materials: A tracking-free determination of the frequency-dependent loss and storage moduli. *Phys. Rev. Mater.* **2017**, *1*, No. 073804.
- (26) Cerbino, R.; Giavazzi, F.; Helgeson, M. E. Differential dynamic microscopy for the characterization of polymer systems. *J. Polym. Sci.* **2021**, No. 1093.
- (27) Martineau, R. L.; Bayles, A. V.; Hung, C.-S.; Reyes, K. G.; Helgeson, M. E.; Gupta, M. K. Engineering Gelation Kinetics in Living Silk Hydrogels by Differential Dynamic Microscopy Microrheology and Machine Learning. *Adv. Biol.* **2021**, No. e2101070.
- (28) Hill, L. K.; Meleties, M.; Katyal, P.; Xie, X.; Delgado-Fukushima, E.; Jihad, T.; Liu, C.-F.; O'Neill, S.; Tu, R. S.; Renfrew, P. D.; Bonneau, R.; Wadghiri, Y. Z.; Montclare, J. K. Thermoresponsive Protein-Engineered Coiled-Coil Hydrogel for Sustained Small Molecule Release. *Biomacromolecules* 2019, 20, 3340–3351.
- (29) Meleties, M.; Katyal, P.; Lin, B.; Britton, D.; Montclare, J. K. Self-assembly of stimuli-responsive coiled-coil fibrous hydrogels. *Soft Matter* **2021**, *17*, 6470–6476.
- (30) Strable, E.; Prasuhn, D. E., Jr.; Udit, A. K.; Brown, S.; Link, A. J.; Ngo, J. T.; Lander, G.; Quispe, J.; Potter, C. S.; Carragher, B.;

- Tirrell, D. A.; Finn, M. G. Unnatural amino acid incorporation into virus-like particles. *Bioconjugate Chem.* **2008**, *19*, 866–875.
- (31) Durresne, E. R.; Squires, T. M.; Brenner, M. P.; Grier, D. G. Hydrodynamic Coupling of Two Brownian Spheres to a Planar Surface. *Phys. Rev. Lett.* **2000**, *85*, 3317–3320.
- (32) O'Neill, S. C.; Bhuiyan, Z. H.; Tu, R. S. Evolution of mechanics in  $\alpha$ -helical peptide conjugated linear- and star-block PEG. *Soft Matter* **2017**, *13*, 7521–7528.
- (33) Pelletier, V.; Gal, N.; Fournier, P.; Kilfoil, M. L. Microrheology of Microtubule Solutions and Actin-Microtubule Composite Networks. *Phys. Rev. Lett.* **2009**, *102*, No. 188303.
- (34) Sathaye, S.; Mbi, A.; Sonmez, C.; Chen, Y.; Blair, D. L.; Schneider, J. P.; Pochan, D. J. Rheology of peptide- and protein-based physical hydrogels: Are everyday measurements just scratching the surface? *Wiley Interdiscip. Rev.: Nanomed. Nanobiotechnol.* **2015**, 7, 34–68.
- (35) Crocker, J. C.; Grier, D. G. Methods of Digital Video Microscopy for Colloidal Studies. *J. Colloid Interface Sci.* **1996**, 179, 298–310.
- (36) Schultz, K. M.; Anseth, K. S. Monitoring degradation of matrix metalloproteinases-cleavable PEG hydrogels via multiple particle tracking microrheology. *Soft Matter* **2013**, *9*, 1570–1579.
- (37) Adolf, D.; Martin, J. E. Time-cure superposition during crosslinking. *Macromolecules* **1990**, 23, 3700–3704.
- (38) Bayles, A. V.; Squires, T. M.; Helgeson, M. E. Dark-field differential dynamic microscopy. *Soft Matter* **2016**, *12*, 2440–2452.
- (39) Bayles, A. V.; Squires, T. M.; Helgeson, M. E. Probe microrheology without particle tracking by differential dynamic microscopy. *Rheol. Acta* **2017**, *56*, 863–869.
- (40) Larsen, T.; Schultz, K.; Furst, E. M. Hydrogel microrheology near the liquid-solid transition. *Korea-Australia Rheol. J.* **2008**, *20*, 165–173.
- (41) Schultz, K. M.; Baldwin, A. D.; Kiick, K. L.; Furst, E. M. Gelation of covalently cross-linked PEG-heparin hydrogels. *Macromolecules* **2009**, *42*, 5310–5316.
- (42) Winter, H. H.; Chambon, F. Analysis of linear viscoelasticity of a crosslinking polymer at the gel point. *J. Rheol.* **1986**, *30*, 367–382.
- (43) Bilge, A. H.; Pekcan, O. A mathematical characterization of the gel point in sol-gel transition. *J. Phys.: Conf. Ser.* **2015**, *574*, No. 012005.
- (44) Winter, H. H. Can the gel point of a cross-linking polymer be detected by the G'-G'' crossover? *Polym. Eng. Sci.* **1987**, 27, 1698–1702.
- (45) Kegel, W. K.; van Blaaderen, A. Direct observation of dynamical heterogeneities in colloidal hard-sphere suspensions. *Science* **2000**, 287, 290–293.
- (46) Oppong, F. K.; Coussot, P.; de Bruyn, J. R. Gelation on the microscopic scale. *Phys. Rev. E* 2008, 78, No. 021405.
- (47) Furst, E. M.; Squires, T. M. Microrheology; Oxford University Press, 2017.
- (48) Khan, M.; Mason, T. G. Local collective motion analysis for multi-probe dynamic imaging and microrheology. *J. Phys.: Condens. Matter* **2016**, 28, No. 305201.
- (49) Richards, J. A.; Martinez, V. A.; Arlt, J. Particle sizing for flowing colloidal suspensions using flow-differential dynamic microscopy. *Soft Matter* **2021**, *17*, 3945–3953.
- (50) Edera, P.; Brizioli, M.; Zanchetta, G.; Petekidis, G.; Giavazzi, F.; Cerbino, R. Deformation profiles and microscopic dynamics of complex fluids during oscillatory shear experiments. *Soft Matter* **2021**, 17, 8553–8566.
- (51) Varanko, A. K.; Su, J. C.; Chilkoti, A. Elastin-Like Polypeptides for Biomedical Applications. *Annu. Rev. Biomed. Eng.* **2020**, 22, 343–369.